ORIGINAL ARTICLE

Certain doping concentrations caused half-metallic graphene

Lu Miao [a], **Ran Jia** [a,*], **Yu Wang** [a], **Chui-Peng Kong** [a], **Jian Wang** [a],
Roberts I. Eglitis [b], **Hong-Xing Zhang** [a,*]

[a] *Institute of Theoretical Chemistry, Jilin University, 130023 Changchun, PR China*
[b] *Institute of Solid State Physics, University of Latvia, 8 Kengaraga Str., Riga LV1067, Latvia*

Abstract   The singly B and N doped graphene systems are carefully studied. The highly concentrated dopants cause a spin polarization effect in the systems. The spin polarization limits are affirmed in the singly B and N doped graphene systems through periodic hybrid density functional theory studies. The spin polarization effects must be considered indeed in the B and N doped graphene systems if the dopant concentration is above 3.1% and 1.4%, respectively. The system symmetry cooperating with the presence of the spin polarization brings half-metallic properties into the doping systems. The semiconducting channels in the half-metallic systems are in two different spin directions due to the different electron configurations of the B and N dopants in graphene.

© 2016 King Saud University. Production and hosting by Elsevier B.V. This is an open access article under the CC BY-NC-ND license (http://creativecommons.org/licenses/by-nc-nd/4.0/).

1. Introduction

As one of the most popular topics at the moment, graphene attracts extensive studies for its unique electronic and mechanical properties [1–5]. It has the same electron configuration as the graphite. The sp^2 hybrid orbitals connect the carbon atoms with each other. The remaining non-hybrid 2p orbitals are perpendicular to the graphene and form a delocalized π-orbital together. The Dirac cone in the band structure of the graphene leads to a massless quasiparticle and a zero band gap in the ordinary state [2]. Hence, it exhibits the excellent electronic properties, such as the high conductivity [6,7], the quantum Hall effect in room temperature [8,9], and so on. Moreover, some external atoms, molecules or clusters can easily be adsorbed on the graphene [10–14] and carbon nanotubes [15–18], owing to the free electrons on the delocalized π-orbital. In some cases, the π-orbital could hybridize with the d-orbitals of its substrate atoms [19–22].

The unique zero band gap of the graphene could be a primary obstacle in the way of its practical applications. Thus, it's crucial for graphene to induce a band gap [23]. The gap can be opened in many ways. A narrow graphene ribbon can bring an energy gap at K and K' points in the Brillouin-zone owing to the lateral confinement of the charge carriers [24]. Castro's experiments and theoretical studies have proved that an applied electric field can adjust the band gap of the bilayer

* Corresponding authors. Tel.: +86 431 8849 8966.
E-mail addresses: jiaran@jlu.edu.cn (R. Jia), zhanghx@jlu.edu.cn (H.-X. Zhang).
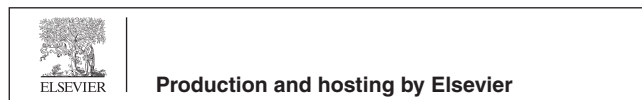
graphene system from zero to the mid-infrared energy region [25]. The strain within the single layer graphene investigated by Ni and his co-workers can bring a 300 meV band gap [26]. With the help of the external electric field, a tunable band gap for the dual-gate bilayer graphene can be opened in the range of 0–250 meV [27].

Recently, the graphene is suggested as a basic substance of the van der Waals heterostructure material by Geim and Grigorieva [28]. The atomic-scale "Lego" expands the application scope of the two-dimensional materials. Self-assembled graphene via multiple-step processes has been studied a lot for its novel structures and functionalities [29]. Wang and his co-workers employed the graphene as a conductive additive in the self-assembled TiO_2–graphene hybrid nanosystem to enhance the insertion/extraction of the Lithium ion in TiO_2 [30]. Xiao et al. have demonstrated a self-assembly method to construct the multilayered film containing the well-defined Quantum Dots/Graphene Nanosheets [31].

In practical cases, the graphene always contains kinds of defects, such as vacancies and impurities. Moreover, introducing the artificially defects is a way to open the band gap of graphene. It could also be a new pretreatment method for the self-assembled hybrid graphene systems. The defects within the graphene layers can interact with each other, so as to affect the assembly process. Therefore, the researches about the defect graphene systems are meaningful and indispensable. The boron (B), nitrogen (N), oxygen (O), sulfur (S), fluoride (F) and phosphorus (P) atoms are the common dopants in graphene, which have the similar van der Waals radius compared with the carbon (C) atom.

The heteroatoms can also change the other electrical properties of graphene. For example, graphene becomes p- or n-type semiconductor by doping with B- or N-atom, respectively [32–34]. Using arc discharge method, the B- and N-doped graphene can be directly synthesized with B_2H_6 and NH_3 or pyridine as the boron and nitrogen sources, respectively [35]. Wu et al. have studied the magnetic behaviors of graphene with adsorbed N-, O- and F-atoms [11]. In their work, a 0.84 μB magnetic moment has been detected in the graphene system with N adsorption, while the adsorbed O- and F-atoms cannot induce any magnetic moment. The geometries, electronic structures and magnetic properties of the light non-metallic atoms doped graphene have also been studied in their subsequent work [36]. They claimed that the dopants like N-, O-, B- and F-atoms could induce a band gap near the Dirac point. Furthermore, only F-atom can induce a 0.71 μB magnetic moment in graphene. Whereas, the graphene systems doped by the other three dopants present no magnetic nature. Zhou et al. [37] have introduced a general 3N rule to describe the size dependence of the electronic properties of the doped graphene. In short, a zero gap appears at Dirac point if the size of the primitive cell of the doped graphene is 3N times of the perfect graphene unit cell. Otherwise, there is a gap. Almost at the same time, Muhich et al. [38] revealed the nature of the non-spin polarized N and B dopant structures in graphene and explained the origins of their n- and p-type semiconduction, respectively. Zeng et al. [39] used B_2C graphene to modify the electron distribution in graphene. Thereby, the Li-atom can be localized on the graphene surface as potential hydrogen storage medium.

However, there are few researches talking about the spin polarization properties of the doped graphene systems. In this work, we want to discuss the spin polarization of the singly B and N doping in the graphene systems. The dopant concentrations are the key point of the appearing spin polarization in doped graphene. Therefore, different concentrations of the B- and N-dopants in graphene are studied carefully in order to find the spin polarization limits. This work is organized as follows: In Section 2, the simulation methods and models are introduced; In Section 3, the calculation results will be presented and discussed; In Section 4, a short conclusion will be given out.

2. Computational methods and details

The calculations, in this work, are carried out using the hybrid Becke-type three-parameter exchange functional [40] combined with the gradient-corrected Lee–Young–Parr correlation functional [41], namely B3LYP, which is fully implemented in the computer code CRYSTAL14 [42]. The basis sets are chosen at Triple-Zeta Valence with Polarization (TZVP) level for all related species (i.e., the B, N and C atoms), which are introduced by Peintinger and coworkers [43]. A 500 Å vacuum, which is automatically inserted into the 2D system by CRYSTAL14, ensures the spatial independence of the single layer graphene sheet. To investigate the spin polarization effects of the doped monolayer graphene, the size of the in-plane supercell increases from 2×2 to 8×8, gradually. Experimentally, an 8.9% N-doping on graphene has been synthesized by chemical vapor deposition [33]. Therefore, the doping sizes in this work are reasonable. A sketch for a 3×3 substituted graphene is illustrated in Fig. 1(a) as an example. To hold the in-plane homogeneity, the systems are two dimensional periodic. Denser substitution, e.g., 1×1 system, is not considered in this work because of its thermodynamic instability according to the research by Shi [44]. The sampling in the two-dimensional Brillouin zone of the supercell for the reciprocal space integrations is performed with the help of an 8×8 Pack–Monkhorst net. With the aid of such relatively sparse net, the Dirac cone can already be reflected in the band structure map for the pristine graphene using CRYSTAL14 (shown in Fig. S1 in the Supporting Information file). Moreover, some dense nets are also tested1, e.g., 16×16, 32×32, 64×64 and 128×128 Pack–Monkhorst nets for perfect monolayer graphene. The deviations among them are less than 0.8 meV. Thus, we believe that the 8×8 Pack–Monkhorst net is good enough to provide reliable results with relatively low time consumption in our research. Both of the spin and non-spin polarized cases are taken into account, in order to identify the stable electronic structures of the doped graphene systems. The thresholds N (i.e., the calculation of integrals with an accuracy of 10^{-N}) for the Coulomb overlap, Coulomb penetration, exchange overlap, the first- and second-exchange pseudo-overlaps are set to 7, 7, 7, 7 and 14.

The pristine structures of the graphite and monolayer graphene are full optimized. It is well known, that a proper dispersion correction is necessary for the description of the interlayer structure in graphite. The pure DFT functionals cannot provide the expected long range r^{-6} type of the London dispersion interaction. Although the focus of the present work is only on the graphene systems, the B3LYP-D2 method is still employed to retain the calculation consistency with the starting point, i.e., the graphite. The dispersion correction parameters for
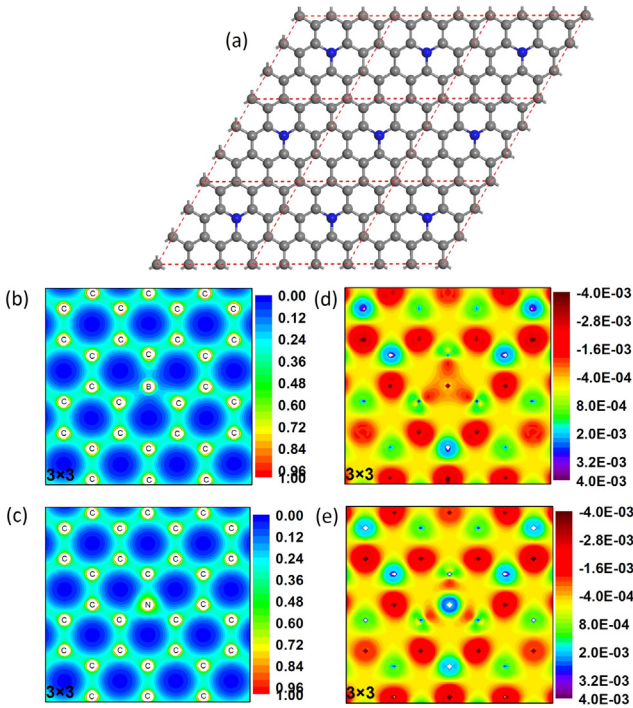
Figure 1 (a) Sketch map for periodic singly atom doping on graphene. The gray balls represent the C atoms, and the blue balls are the B or N dopants. The example system, shown here, is a 3×3 periodic doped monolayer graphene. The system can therefore retain to be in-plane homogeneous; (b) and (c) electron density maps of the spin polarized B and N doping on a monolayer graphene calculated in a 3×3 supercell, respectively. The contours are set between 0 and $1.0 \, e/\text{bohr}^3$ with a linear spacing of $0.04 \, e/\text{bohr}^3$; (d) and (e) spin density maps of the spin polarized B and N doping in monolayer graphene calculated in a 3×3 supercell. The spin density contours are varied from -0.004 to $0.004 \, e/\text{bohr}^3$ with a linear spacing of $0.0002 \, e/\text{bohr}^3$.

D2 method are based on the suggestions in the original work by Grimme [45]. In particular, the dispersion coefficients C_6 are set to the suggested values in Grimme's work [46]. The van der Waals Radii R_0 are adjusted as 2.21 Å, 1.92 Å and 1.55 Å for C-, B- and N-atoms, respectively. After the full geometry optimization for graphite, a 3.24 Å interlayer distance is obtained, which has a deviation around 3% from the experimental value 3.35 Å [47]. Our calculated bond length between the in-plane C-atoms is 1.41 Å, while the experimental value is 1.42 Å. The deviation between them is barely 0.7%. For the other atoms involved in our study, the hexagonal boron nitride (h-BN) has also been simulated. Using the corresponding correction parameters, a 3.33 Å interlayer distance in h-BN is obtained. Apparently, the method used in this study is valid and reliable. Note that the modeling systems are fully optimized during the simulations. For the doped graphene, the dispersion correction term is not necessary. However, this term is retained in the simulations as a precaution to keep the consistency in the whole research.

The effective charges and overlap populations between the nearest neighbors are obtained using the standard Mulliken analysis.

3. Results and discussion

In order to compare the stabilities of the spin and non-spin polarized structures, the energy difference between the corresponding doped systems is defined as follows:

$$\Delta E(m : X) = E_{\text{spin}}(m : X) - E_{\text{non-spin}}(m : X), \quad (1)$$

where m denotes the $m \times m$ supercell and X refers to the B- or N-atom dopants. The negative ΔE indicates that the corresponding system is spin polarized. Otherwise, the system should be non-spin polarized.

3.1. Boron doping

A single B-atom as dopant replaces a C-atom in the supercell which is varied from 2×2 to 8×8 in this research. Therefore, the concentration of the B-impurity in graphene decreases from 12.5% to 0.7%. The energy differences between the spin and non-spin polarized systems for the B doped graphene are listed in Table 1. Because a free B-atom lacks one electron than the C-atom, the doped graphene system with an isolated B dopant would have an unpaired electron. However, when the concentration of the B-dopant is under 3.1%, the energy differences demonstrate that the system is non-spin polarized, though the differences display only a few meV. On the contrary, if the dopant concentration reaches 3.1% or even higher, the system turns to spin polarized. The effective charges of the B-dopants in spin and non-spin polarized systems are exhibited in Table 1. The B-atoms as impurities in the systems lose around 650 me charges, compared with the free B-atoms. The lost charges are distributed almost averagely on the first three C-neighbors around the impurity centers. For the second and other far neighbors, their total effective charges can be

Table 1 The total effective charges and charge differences on the dopants, and the energy differences between the spin and non-spin polarized systems at relative dopant concentrations. $n_{\alpha+\beta} = n_\alpha + n_\beta$ and n denote the total effective charges located on the B or N dopants, where n_α and n_β are the effective charges with different spin directions. Similarly, the charge difference is defined as $n_{\alpha-\beta} = n_\alpha - n_\beta$. ΔE represents the energy difference between the spin and non-spin polarized systems calculated from Eq. (1).

	Concentration [%]	Spin $n_{\alpha+\beta}$[e]	$n_{\alpha-\beta}$[e]	Non-spin n[e]	ΔE [meV]
B doping	0.7	0.642	0.082	0.637	35.9
	1.0	0.643	0.101	0.639	7.1
	1.4	0.648	0.136	0.638	7.8
	2.0	0.646	0.113	0.639	3.7
	3.1	0.649	0.144	0.641	−35.9
	5.6	0.656	0.178	0.639	−126.9
	12.5	0.658	0.156	0.642	−204.9
N doping	0.7	−0.601	0.074	−0.590	103.7
	1.0	−0.605	0.094	−0.592	135.6
	1.4	−0.613	0.134	−0.593	−102.5
	2.0	−0.609	0.110	−0.600	−66.7
	3.1	−0.617	0.144	−0.600	98.3
	5.6	−0.626	0.177	−0.602	−201.5
	12.5	−0.620	0.160	−0.602	−226.9

regarded as the same as before in the perfect graphene. The charge transfer stems from the higher electron affinity of C-atom. The short range charge transfer indicates that the electrons on B are distributed mostly through three B–C sp^2 σ-bonds. The effective charge on the B-atom keeps increasing with the cutting down of the dopant concentration. The electron and spin density maps of the spin polarized B-dopant in the 3×3 periodic system are illustrated in Fig. 1(b) and (d). And the electron density maps for the B doping systems with other B concentrations can also be found in Fig. S2 in the Supporting Information file. Now, the electron deficiency is visualized in the plot of the electron density map in Fig. 1(b). One can also find the spin density map for spin polarized B doped 3×3 periodic system, which showing the performance of the spin density in the doping region is notably different from the perfect part. Other spin density maps are illustrated as Fig. S3 in the Supporting Information. The electron differences between two spin directions on B are between 140 and 180 me in 2×2, 3×3 and 4×4 periodic doping systems. The electron overlap population (EOP) between the nearest C-atoms in undoped graphene is calculated to be 451 me in current work. The contours between B and C shown in the density maps are sparser than them between the C-atoms. It also indicates that the EOPs between B- and its first order C-atoms in all of the doped systems, no matter whether it is spin polarized or non-spin polarized, are slightly less than this value. However, the decrease of B concentration leads to an increasing EOP. In the systems with low B impurity concentrations, the EOPs are almost identical with the pristine C–C value. This changing trend implies that the interaction between B and its first neighbor is strengthened, and the B dopant is more and more similar to the substituted C-atom in a low concentrated system. Therefore, in the relative low concentration system, the B doped graphene shows non-spin polarized. The details of EOP values between B and C in the spin and non-spin polarized B doping systems are listed in Table S1.

Owing to the charge re-distribution, the bond length between the B- and C-atoms changes as well. Due to the electron transfer from B to C, the σ-bond orbitals between them distort toward the C-atoms. Therefore, the B–C bond lengths are around 5% longer than the distance between the nearest C-atoms in perfect graphene. The B–C bond length decreases monotonically with the decreasing B concentration and converges to 1.48 Å. A local distortion in graphene, for example, the Stone–Wales defects, causes the re-manipulation of the band structure [37,47]. This re-manipulation appears in our investigated hybrid systems, too. Our calculated band structures for the non-spin polarized B doped graphene systems (shown in Fig. 3) represent the so-called 3N rule from 2×2 to 8×8 as mentioned in Zhou's work [37]. However, based on the information obtained from the energy differences between the spin and non-spin polarized calculations, the spin polarization should be taken into account for the B doped graphene from 2×2 to 4×4. The spin polarized band structures of the B doped systems are presented in Fig. 2. The other non-spin polarized band maps are illustrated in Fig. 3. The Fermi levels are dropped into the valance bands for both spin and non-spin polarized cases, so that the B doped graphene acts as a p-type semiconductor. In spin polarized 2×2 and 4×4 hybrid systems, α- and β-maps show obvious difference from each other in the vicinity of the band gaps. Note that we use α and β to distinguish two different spin directions of the
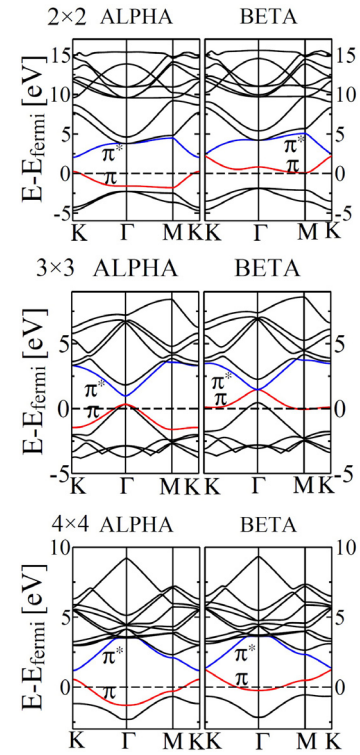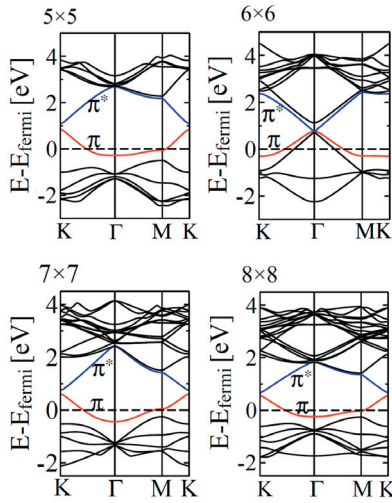

Figure 2 Band structures for the spin polarized B doped graphene systems with high dopant concentrations at 12.5%, 5.6% and 3.1%, i.e., the supercell sizes are 2×2, 3×3 and 4×4, respectively. The dashed lines in the maps point out the Fermi-levels. Note that all of the Fermi-levels are shifted to zero. The high symmetry points in the first Brillouin-zone are set as follows: $\Gamma = (0,0,0)$, $K = (\frac{1}{3}, \frac{1}{3}, 0)$, $M = (0, \frac{1}{2}, 0)$. Also note that the "ALPHA" and "BETA" over every panel indicates the different spin directions of the band maps, respectively.
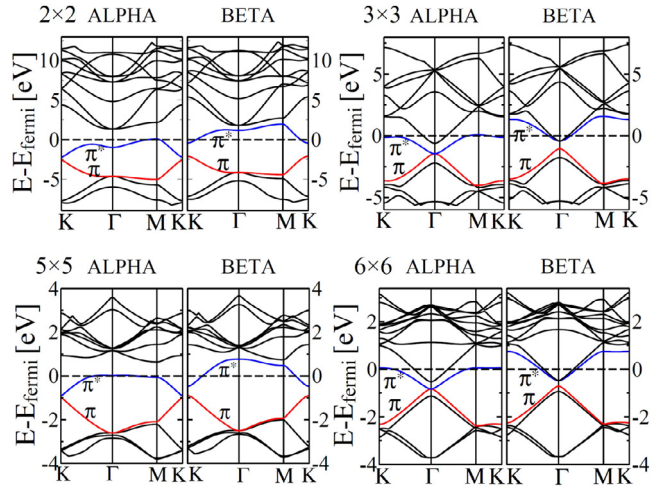
electron, namely spin up and down, or with other words, the majority and minority spin channels. In β direction, the band gaps at high symmetric point K are far narrower than that in α direction. More importantly, there is no gap in β band map for 3×3 doped graphene system, but a clear direct gap (i.e., $E_{gap}(\alpha) = 650$ meV as shown in Fig. 2) exists at Γ point in α map. It means that the B doped 3×3 graphene is a half-metallic material, not exactly like the conclusion in a previous research [37]. Considering that, the spin polarization becomes particularly important in this situation. The calculated band gaps are listed in the first part of Table 2 for both spin and non-spin polarized cases.

3.2. Nitrogen doping

Similar to the B doping, the simulated primitive cells are also varied from 2×2 to 8×8. The effective charges of the N dopants and energy differences between the spin and non-spin calculations for different N doping concentrations are listed in Table 1, too. From the perspective of the energy, the spin polarized N doping on graphene is more stable than the non-spin polarized one, when the doping concentration is higher than 1.0%. One exception is the system with the concentration 3.1%. Its energy difference presents a stable non-spin polarized N doped system. As same as the free B atom,

Figure 3 Band structures for the non-spin polarized B doped graphene systems with relative low dopant concentrations at 2.0%, 1.4%, 1.0%, and 0.7%, i.e., the supercell sizes are chosen from 5×5 to 8×8, respectively. The dashed lines in the maps point out the Fermi-levels. Note that all of the Fermi-levels are shifted to zero. The high symmetry points in the first Brillouin-zone are set as follows: $\Gamma = (0, 0, 0)$, $K = (\frac{1}{3}, \frac{1}{3}, 0)$, $M = (0, \frac{1}{2}, 0)$. Also note that the "ALPHA" and "BETA" over every panel indicates the different spin directions of the band maps, respectively.

Table 2 The direct band gaps at high symmetry point in the first Brillouin-zone of the B and N doped graphene systems. The columns denoted by α and β list the values of the band gaps in the band structure maps with two spin directions. The non-spin polarized band gaps are named directly as "non-spin".

Concentration [%]	B doping [meV]			N doping [meV]		
	α	β	Non-spin	α	β	Non-spin
0.7	205.8	67.0	127.4	69.8	175.1	107.7
1.0	264.0	75.1	149.4	82.5	223.8	132.2
1.4	240.6	0	0	0	237.4	0
2.0	344.6	252.7	252.9	103.7	418.1	228.1
3.1	638.3	144.6	331.2	145.4	597.7	304.1
5.6	650.6	0	0	0	642.2	0
12.5	1794.2	324.6	920.8	401.3	1678.9	926.3

the free N atom has also an unpaired electron. However, the N atom has an extra electron with respect to C. In this regard, the N and B doping on graphene should show great differences of the electronic properties. Different with B doping, N acts as an electron "acceptor" in the doped systems, while B acts as a "donor". The substituting N atom gains around 610 me charges from its first neighboring C-atoms through the sp^2 σ-bonds. Taking the electron density distribution of the 3×3 doped system shown in Fig. 1(c) as an example, the contours surrounding the N-dopant are much denser than that in other regions because of the electron acceptance. The accepted charges decrease generally with the decreasing N concentration in system. However, the 3×3 and 6×6 systems show two local minima, exactly corresponding to the 3N rule. The spin density map in Fig. 1(e) shows that the spin difference is mainly located in a concentrated area centering on N, not like the B doping, in which spin difference contours near by the

Figure 4 Band structures for the spin polarized N doped graphene systems with high dopant concentrations at 12.5%, 5.6%, 2.0% and 1.4%, i.e., the supercell sizes are chosen as 2×2, 3×3, 5×5 and 6×6, respectively. The dashed lines in the maps point out the Fermi-levels. Note that all of the Fermi-levels are shifted to zero. The high symmetry points in the first Brillouin-zone are set as follows: $\Gamma = (0, 0, 0)$, $K = (\frac{1}{3}, \frac{1}{3}, 0)$, $M = (0, \frac{1}{2}, 0)$. Also note that the "ALPHA" and "BETA" over every panel indicates the different spin directions of the band maps, respectively.

B-dopant are widely dispersed. The spin difference values are also listed in Table 1. The generally decreasing spin difference with the reduction of the dopant concentration indicates that the N doped graphene system should be non-spin polarized at a low dopant concentration. The other electron and spin density maps are illustrated in the Supporting Information file as Figs. S4 and S5.

Due to the charge re-distribution, the EOP and bond length between N and its first neighbors are changed similarly as in aforementioned B doped graphene. The EOPs between N and its first neighbors are about 13% to 17% less than 451 me, which are the EOPs between C-atoms in pristine graphene. The relative sparse electron density contours in Fig. 1(c) confirm the EOP lost between N and C. Moreover, they are around 60 me weaker than that in the corresponding B doped graphene systems. The increasing trend is retained with the decreasing dopants concentration as it is in the B doped graphene systems. It implies that the N–C covalent bonds are weaker than the B–C bonds. Surprisingly, the N–C bonds are much shorter than B–C bonds, and very close to the pristine C–C bond length. In the low concentration systems, the N–C bonds are even slightly shorter than the pristine C–C bond, according to our non-spin polarized simulations. More details can be found in the Table S2 in the Supporting Information. However, the σ-bond orbitals lean toward the N dopants. Consequently, the N–C bond becomes shorter than that between B and C. The shifts of the σ-bond orbitals between N and C can also be observed via the electron density contour map in Fig. 1(c).

Similarly to the B doping, the non-spin polarized band structures of the N doped graphene systems obey the 3N rule. The calculated band gaps in the spin and non-spin polarized N doped graphene systems are listed in Table 2. The spin and non-spin polarized band structures are presented in Figs. 4
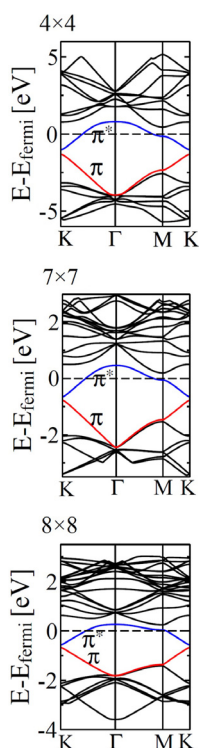
Figure 5 Band structures for the non-spin polarized N doping in graphene systems with relative low dopant concentrations at 3.1%, 1.0% and 0.7%, i.e., the supercell sizes are set to 4×4, 7×7 and 8×8, respectively. The dashed lines in the maps point out the Fermi-levels. Note that all of the Fermi-levels are shifted to zero. The high symmetry points in the first Brillouin-zone are set as follows: $\Gamma = (0, 0, 0)$, $K = (\frac{1}{3}, \frac{1}{3}, 0)$, $M = (0, \frac{1}{2}, 0)$. Also note that the "ALPHA" and "BETA" over every panel indicates the different spin directions of the band maps, respectively.

and 5, respectively. The N doped graphene systems act as an n-type semiconductor, whose Fermi-levels are shifted up into the conduction bands, in contrast to the B doping. Due to the feature of the energy stability, the singly N doping on graphene should be considered to be spin polarized when the dopant concentration is higher than 1.0% as mentioned above. For the spin polarized cases, the α- and β-maps show great differences near the Fermi-levels, as before. The most obvious difference is that the band gaps in α direction are far narrower than the β-gaps, which is just the opposite of the B doping cases. The α-maps still obey the 3N rule. There is no gap showing in the high symmetric point Γ in the α-maps if the primitive size of the supercell is $3N \times 3N$. In the meantime, a clear gap always shows in β-map. It means that the singly N doped graphene systems at these concentrations are not semiconductors or metals, but half-metallic materials. Based on the information obtained all above, taking the spin polarization into account becomes significantly important in these situations. The gaps show a general decreasing trend with the cutting down of the dopant concentration, just like the B doping.

4. Conclusion

The spin polarization effects of the singly B and N doped graphene systems were studied using the B3LYP method.

Unlike the metallic pristine graphene, the spin effects in a semiconducting system should be taken into account, because the linear relationship between the energy and momentum no longer exists, and the electron mobility could be greatly changed. The spin polarization must be tested before studying the electronic properties of the singly substitution structures of graphene, if the dopant concentration is higher than 1.4%. Most recently, the experimental results about the N and B superdoping of graphene are reported by Liu and his co-workers [48]. They claimed that the N superdoping of graphene can induce ferromagnetism and the doping concentration is an important factor. These results could strongly support our research. The $3N \times 3N$ doping systems with high dopant concentrations show the half-metallic properties instead of metallic. This detailed understanding of the spin polarization effects could be very important for the further developments of the electronic devices with graphene. The half-metallic graphene has a high technological potential in the field of the spintronics, for example, the electron-spin filter.

Acknowledgment

Appendix A. Supplementary data

Supplementary data associated with this article can be found, in the online version, at http://dx.doi.org/10.1016/j.jscs.2016.03.007.

References

[1] K.S. Novoselov, S.V. Morozov, D. Jiang, Electric field effect in atomically thin carbon films, Science 306 (2004) 666–669.

[2] K.S. Novoselov, A.K. Geim, S.V. Morozov, D. Jiang, M.I. Katsnelson, I.V. Grigorieva, S.V. Dubonos, A.A. Firsov, Two-dimensional gas of massless Dirac fermions in graphene, Nature 438 (2005) 197–200.

[3] Y. Zhang, Y.W. Tan, H.L. Stormer, P. Kim, Experimental observation of the quantum Hall effect and Berry's phase in graphene, Nature 438 (2005) 201–204.

[4] C. Berger, Z.M. Song, X.B. Li, X.S. Wu, N. Brown, C. Naud, D. Mayou, T.B. Li, J. Hass, A.N. Marchenkov, E.H. Conrad, P.N. First, W.A. de Heer, Electronic confinement and coherence in patterned epitaxial graphene, Science 312 (2006) 1191–1196.

[5] B. Özyilmaz, P.J. Herrero, D. Efetov, P. Kim, Electronic transport in locally gated graphene nanoconstrictions, Appl. Phys. Lett. 91 (2007) 192107.

[6] A.K. Geim, K.S. Novoselov, The rise of graphene, Nat. Mater. 6 (2007) 183–191.

[7] A.A. Balandin, S. Ghosh, W. Bao, I. Calizo, D. Teweldebrhan, F. Miao, C.N. Lau, Superior thermal conductivity of single-layer graphene, Nano Lett. 8 (2008) 902–907.

[8] N. Gorjizadeh, Y. Kawazoe, Chemical functionalization of graphene nanoribbons, J. Nanomater. 7 (2010) 513501.

[9] C.L. Kane, E.J. Mele, Quantum spin hall effect in graphene, Phys. Rev. Lett. 95 (2005) 226801.

[10] Y. Zhou, X. Zu, F. Gao, H. Xiao, H. Lv, Electronic and magnetic properties of graphene absorbed with S atom: a first-principles study, J. Appl. Phys. 105 (2009) 104311.

[11] M. Wu, E. Liu, J. Jiang, Magnetic behavior of graphene absorbed with N, O, and F atoms: a first-principles study, Appl. Phys. Lett. 93 (2008) 082504.

[12] Y. Zhou, X. Zu, F. Gao, H. Lv, H. Xiao, Adsorption-induced magnetic properties and metallic behavior of graphene, Appl. Phys. Lett. 95 (2009) 123119.

[13] G. Kim, S.H. Jhi, Ca-decorated graphene-based three-dimensional structures for high-capacity hydrogen storage, J. Phys. Chem. C 113 (2009) 20499–20503.

[14] Y. Li, G. Zhao, C. Liu, Y. Wang, J. Sun, Y. Gu, Y. Wang, Z. Zeng, The structural and electronic properties of Li-doped fluorinated graphene and its application to hydrogen storage, Int. J. Hydrogen Energy 37 (2012) 5754–5761.

[15] Z. Fang, S. Li, Y. Gong, W. Liao, S. Tian, C. Shan, C. He, Comparison of catalytic activity of carbon-based AgBr nanocomposites for conversion of CO_2 under visible light, J. Saudi Chem. Soc. 18 (2014) 299–307.

[16] I. Mobasherpour, E. Salahi, M. Ebrahimi, Thermodynamics and kinetics of adsorption of Cu(II) from aqueous solutions onto multi-walled carbon nanotubes, J. Saudi Chem. Soc. 18 (2014) 792–801.

[17] C.L. Phillips, C.S. Yah, S.E. Iyuke, K. Rumbold, V. Pillay, The cellular response of *Saccharomyces cerevisiae* to multi-walled carbon nanotubes (MWCNTs), J. Saudi Chem. Soc. 19 (2015) 147–154.

[18] H.A. Asmaly, B. Abussaud, Ihsanullah, T.A. Saleh, V.K. Gupta, M.A. Atieh, Ferric oxide nanoparticles decorated carbon nanotubes and carbon nanofibers: from synthesis to enhanced removal of phenol, J. Saudi Chem. Soc. 19 (2015) 511–520.

[19] C. Gong, G. Lee, B. Shan, E.M. Vogel, R.M. Wallace, K. Cho, First-principles study of metal–graphene interfaces, J. App. Phys. 108 (2010) 123711.

[20] D. Zhao, G. Sheng, C. Chen, X. Wang, Enhanced photocatalytic degradation of methylene blue under visible irradiation on graphene@TiO_2 dyade structure, Appl. Catal. B 111–112 (2012) 303–308.

[21] P.K. Gogoi, P.E. Trevisanutto, M. Yang, I. Santoso, T.C. Asmara, A. Terentjevs, F.D. Sala, M.B.H. Breese, T. Venkatesan, Y.P. Feng, K.P. Loh, A.H.C. Neto, A. Rusydi, Optical conductivity renormalization of graphene on $SrTiO_3$ due to resonant excitonic effects mediated by Ti 3d orbitals, Phys. Rev. B 91 (2015) 035424.

[22] R. Requist, P.M. Sheverdyaeva, P. Moras, S.K. Mahatha, C. Carbone, E. Tosatti, Spin-orbit interaction and Dirac cones in d-orbital noble metal surface states, Phys. Rev. B 91 (2015) 045432.

[23] S.Y. Zhou, G.-H. Gweon, A.V. Fedorov, P.N. First, W.A. De Heer, D.-H. Lee, F. Guinea, A.H. Castro Neto, A. Lanzara, Substrate-induced bandgap opening in epitaxial graphene, Nat. Mater. 6 (2007) 770–775.

[24] M.Y. Han, B. Özyilmaz, Y. Zhang, P. Kim, Energy band-gap engineering of graphene nanoribbons, Phys. Rev. Lett. 98 (2007) 206805.

[25] E.V. Castro, K.S. Novoselov, S.V. Morozov, N.M.R. Peres, J.M.B. Lopes dos Santos, J. Nilsson, F. Guinea, A.K. Geim, A.H. Castro Neto, Biased bilayer graphene: semiconductor with a gap tunable by the electric field effect, Phys. Rev. Lett. 99 (2007) 216802.

[26] Z. Ni, T. Yu, Y. Lu, Y. Wang, Y. Feng, Z. Shen, Uniaxial strain on graphene: Raman spectroscopy study and band-gap opening, ACS Nano 2 (2008) 2301–2305.

[27] Y. Zhang, T. Tang, C. Girit, Z. Hao, M.C. Martin, A. Zettl, M.F. Crommie, Y.R. Shen, F. Wang, Direct observation of a widely tunable bandgap in bilayer graphene, Nature 459 (2009) 820–823.

[28] A.K. Geim, I.V. Grigorieva, Van der Waals heterostructures, Nature 499 (2013) 419–425.

[29] Y.X. Xu, K.X. Sheng, C. Li, G.Q. Shi, Self-assembled graphene hydrogel via a one-step hydrothermal process, ACS Nano 4 (2010) 4324–4330.

[30] D.H. Wang, D. Choi, J. Li, Z.G. Yang, Z.M. Nie, R. Kou, D.H. Hu, C.M. Wang, L.V. Saraf, J.G. Zhang, I.A. Aksay, J. Liu, Self-assembled TiO_2–Graphene hybrid nanostructures for enhanced Li-ion insertion, ACS Nano 3 (2009) 907–914.

[31] F.X. Xiao, J.W. Miao, B. Liu, Layer-by-Layer self-assembly of CdS quantum dots/graphene nanosheets hybrid films for photoelectrochemical and photocatalytic applications, J. Am. Chem. Soc. 136 (2014) 1559–1569.

[32] N. Al-Aqtash, K.M. Al-Tarawneh, T. Tawalbeh, L. Vasiliev, Ab initio study of the interactions between boron and nitrogen dopants in graphene, J. Appl. Phys. 112 (2012) 034304.

[33] D.C. Wei, Y.Q. Liu, Y. Wang, H.l. Zhang, L.P. Huang, G. Yu, Synthesis of N-doped graphene by chemical vapor deposition and its electrical properties, Nano Lett. 9 (2009) 1752–1758.

[34] Y.H. Zhang, Y.B. Chen, K.G. Zhou, C.H. Liu, J. Zeng, H.L. Zhang, Y. Peng, Improving gas sensing properties of graphene by introducing dopants and defects: a first-principles study, Nanotechnology 20 (2009) 185504.

[35] L.S. Panchakarla, A. Govindaraj, C.N.R. Rao, Boronand nitrogen-doped carbon nanotubes and graphene, Inorg. Chim. Acta 363 (2009) 4163–4174.

[36] M. Wu, C. Cao, J.Z. Jiang, Light non-metallic atom (B, N, O and F)-doped graphene: a first-principles study, Nanotechnology 21 (2010) 505202.

[37] Y.C. Zhou, H.L. Zhang, W.Q. Deng, A 3N rule for the electronic properties of doped graphene, Nanotechnology 24 (2013) 225705.

[38] C.L. Muhich, J.Y. Westcott IV, T.C. Morris, A.W. Weimer, C.B. Musgrave, The effect of N and B doping on graphene and the adsorption and migration behavior of Pt atoms, J. Phys. Chem. C 117 (2013) 10523.

[39] H. An, C. Liu, Z. Zeng, C. Fan, X. Ju, Li-doped B_2C graphene as potential hydrogen storage medium, App. Phys. Lett. 98 (2011) 173101.

[40] A.D. Becke, Density-functional exchange-energy approximation with correct asymptotic behavior, Phys. Rev. A 38 (1988) 3098.

[41] J.P. Perdew, J.A. Chevary, S.H. Vosko, K.A. Jackson, M.R. Pederson, D.J. Singh, C. Fiolhais, Atoms, molecules, solids, and surfaces: applications of the generalized gradient approximation for exchange and correlation, Phys. Rev. B 46 (1992) 6671.

[42] R. Dovesi, V.R. Saunders, C. Roetti, R. Orlando, C.M. Zicovich-Wilson, F. Pascale, B. Civalleri, K. Doll, N.M. Harrison, I.J. Bush, P. DArco, M. Llunell, M. Causà, Y. Noël, CRYSTAL14 User's Manual, University of Torino, Torino, 2014;
R. Dovesi, R. Orlando, A. Erba, C.M. Zicovich-Wilson, B. Civalleri, S. Casassa, L. Maschio, M. Ferrabone, M. De La Pierre, P. DArco, Y. Noel, M. Causa, M. Rerat, B. Kirtman, CRYSTAL14: a program for the ab initio investigation of crystalline solids, Int. J. Quantum Chem. 114 (2014) 1287–1317.

[43] M.F. Peintinger, D.V. Oliveira, T. Bredow, Consistent Gaussian basis sets of triple-zeta valence with polarization quality for solid-state calculations, J. Comput. Chem. 34 (2013) 451–459.

[44] Z.M. Shi, A. Kutana, B.I. Yakobson, How much N-doping can graphene sustain?, J Phys. Chem. Lett. 6 (2015) 106–112.

[45] S. Grimme, Semiempirical GGA-type density functional constructed with a long-range dispersion correction, J. Comput. Chem. 27 (2006) 1787–1799.

[46] J.W. Anthony, R.A. Bideaux, K.W. Bladh, M.C. Nichols, Handbook of Mineralogy: Volume I. Elements, Sulfides, Sulfosalts, Mineral Data Publishing, Tucson, Arizona, 1990.

[47] S. Shirodkar, U. Waghmare, Electronic and vibrational signatures of Stone–Wales defects in graphene: first-principles analysis, Phys. Rev. B 86 (2012) 165401.

[48] Y. Liu, Y. Shen, L. Sun, J. Li, C. Liu, W. Ren, F. Li, L. Gao, J. Chen, F. Liu, Y. Sun, N. Tang, H. Cheng, Y. Du, Elemental superdoping of graphene and carbon nanotubes, Nat. Comm. 7 (2016) 10921.